Article citation info:
Hameed MR, Ali SA. Hadwan HH, Toman AA, Mahdi MA. CFD-FSI analysis of textured journal bearing working with nano lubricant. Diagnostyka. 2024;25(2):2024212. https://doi.org/10.29354/diag/188391.

DIAGNOSTYKA, 2024, Vol. 25, No. 2

e-ISSN 2449-5220
DOI: 10.29354/diag/188391

CFD-FSI ANALYSIS OF TEXTURED JOURNAL BEARING WORKING WITH NANO LUBRICANT

Mohanad Ramadhan HAMEED [*], **Sarmad Ahmed ALI**, **Hamid Hussain HADWAN**, **Ahmed Ali TOMAN**, **Mushrek A. MAHDI**

University of Babylon, Institution of Engineering/Al-Musayab, Iraq
[*] Corresponding author, e-mail: msb.mohanad.ramadhan@uobabylon.edu.iq

Abstract

This research aims to examine the compound impact of adding rectangular textures to various zones on the surface of the bearing and nanoparticles in the lubricant on the properties of journal bearing. A lubrication models with various texture depths and eccentricity ratios of journal bearing are created and simulated using CFD-FSI method to get static properties like load capacity and frictional force. Aluminum oxide nanoparticles were added in weight ratios ranging from 0.1 to 0.5 %, and the change in viscosity due to these additives in the lubricant was considered. Cavitation and the dependence of viscosity on temperature effects are also considered. The validation results show that the acquired results from the current simulation method agree well with the experimental results in the reference. The outcomes indicated that the highest load capacity and the lowest frictional force are found in the high-pressure region. It was noted that the maximum rise in load capacity was 16.51% without nanoparticles at a texture depth of 0.5 mm and eccentricity ratio of 0.1, and with the adding of 0.5 wt. % of nanoparticles to the lubricant in the same region, the load carrying capacity increased to 40.87 % compared to a bearing without textures.

Keywords: bearing properties, textures, nanoparticles, load carrying capacity, friction force, CFD-FSI

1. INTRODUCTION

Journal bearings (JB) are regularly utilised in turning machines such as manufacturing, automobiles, and other types of machinery. However, high temperatures can negatively affect bearing performance due to the extreme shear rate resulting from high rotation and loads. Texturing the surface of the bearing and additives of nanoparticles to lubricant are methods utilised to improve the performance of JB under severe conditions. Recently, JB performance have been explored under the impact of texture form, height, and position on the bearing surface. Nanoparticle additives to lubricants has emerged interest, as it has shown positive results in increasing pressure spreading, improving load carrying capacity (LCC), and reducing frictional force (FF). Considerable examinations have been conducted to analyse the influence of surface texture parameters and nanoparticle addition in lubricants on the characteristics of JB:

Rao et al. [1] analysed the influence of a partially texturing the surface of the bearing, discovered promising results in LCC, and FF. Ganji et al. [2] experimentally examined the static properties of textured JB with elliptical textures, found the LCC increases as the number of textures increases, compared with the untextured bearing. Shinde et al. [3] examined the static properties of textured JB with cone shaped textures, found an increase in LCC. Many investigators later, Sharma et al. [4], Tala et al. [5], and Buscaglia et al. [6], conducted studies on the influence of using different models of texture on the static properties of JB and noted an improvement in the JB properties. Zhang et al. [7] examined the impact of considering the deformation of textured bearing on its characteristics using a fluid-structural interaction as a tool. Their result shows an improvement in the LCC with the consideration of the bearing deformation. Niu et al. [8] examined the static properties of complete and partial texturing of the surface of the bearings and got better results with partially textured bearings. In addition, Yu et al. [9] examined the impacts of texture and lubricant rheological parameters on the LCC and FF of JB and observed an increase in LCC with appropriate use and placement of the texture. Manser et al. [10] explored the impact of texture parameters on the characteristics of JB and noted that texture parameters have a major impact on the properties of unaligned journals at higher eccentricity ratios (ε). Kango et al. [11] explored the impact of texture parameters on the surface of bearings and noted that textures in the divergence region only of the bearing (second half region) enhanced bearing properties

Received 2023-12-14; Accepted 2024-05-08; Available online 2024-05-23

more than the texturing of the complete bearing surface.

Babu et al. [12] analysed the impact of adding nanoparticles in lubricants by developing a mathematical model to solve the Reynolds equation (RE) by finite element method (FEM) and noted that adding aluminium oxide nanoparticles (AL2O3) improved the static properties of JB. Binu et al. [13] employed the Krieger-Dougherty viscosity method to investigate the effect of Titanium oxide nanoparticles (TiO2) addition and observed an enhancement in LCC in comparison to lubricants without TiO2. Dang et al. [14] explored the static and thermal characteristics of elliptical bearings by adding Copper oxide nanoparticles (CuO) and TiO2 nanoparticles to lubricants with weight fractions Wt. % of 0.5, 1.0, and 2.0 at different ε and speeds, and noted that the LCC improved with the increase in Wt. % of nanoparticles, and there was no significant increase in oil temperature. Sia et al. [15] explored the properties of Silicon dioxide nanoparticles (SiO2) in lubricants in plain bearings with different weight ratios using a surface roughness examiner and observed that the roughness of the surface improved by adding SiO2 with 0.5 wt. % to the lubricant. Gundarneeya et al. [16] explored the impact of adding nanoparticles in Avalon viscosity lubricant at different speeds to enhance the properties of JB and noted significant improvements in maximum pressure and LCC compared to using lubricant without adding nanoparticles. Nair et al. [17] calculated the characteristics of bearings working with nanoparticles by utilising FEM to solve the RE and noted improvement in LCC. Yathish et al. [18] analysed the characteristics of a biaxial groove journal with nanoparticle-filled lubricants, observing an increase in LCC compared to lubricants without additives. Suryawanshi et al. [19] compared the properties of plain and elliptical bearings, where the shear viscosity measurements introduced nanoparticles into the lubricant at different Wt. % of nanoparticles using a Tribo tester indicated improved performance in elliptical bearings compared to the plain bearings. Bhattacharjee et al. [20] explored the impact of lubricant and nanoparticle mixtures on hydrostatic bearings using a modified Darcy flow model and observed an improvement in performance by adding nanoparticles to the lubricant. Sadabadi et al. [21] used a computational approach with discrete modelling to investigate the performance of Nanofluid lubricant IF-WS2 in bearings, and the results showed an increase in LCC.

In view of previous research, researchers extensively used textures with different shapes, sizes, and locations to improve the performance of the JB. Furthermore, nanoparticles were also used as an additive to improve the lubricant's performance. The effect of texture and nanoparticles together on JB properties has not been used in previous research. In the present study, the impact of adding AL2O3 nanoparticles to the base lubricant, combined with a rectangular-shaped texture, on the static properties of JB is investigated utilizing the fluid-structure interaction (FSI) approach. The conservation equations and the elasticity equation are solved numerically using ANSYS fluent and mechanical structure software, respectively. In the analysis, the rectangular texture shape was used on the surface of the bearing, and the influence of the texture depth on the convergence region, high-pressure region, and divergence region was taken into account as a geometric parameter. The viscosity variation due to adding AL2O3 nanoparticles in the lubricant has been calculated at a weight fraction of 0.1-0.5% by employing an experimentally verified regression method. Cavitation and the dependence of viscosity on temperature effects are also considered. The combined investigation covers ε from 0.1 to 0.9.

2. METHODOLOGY

2.1. Model geometry

The computational model comprises two domains: solid (the journal and bearing) and fluid (lubricant). These domains are illustrated in Figure 1. The geometric dimensions and operating conditions were chosen to be as close as possible to those of the JB for the experiment [22].

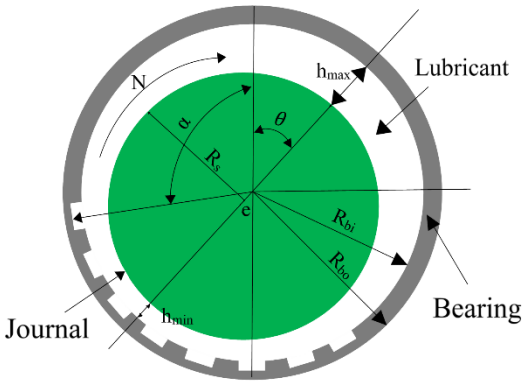

Fig. 1. Geometrical view of hydrodynamic JB

Table 1 depicts the dimensions of the textured JB. The textured region consists of 48 rectangular textures, 8 in tangential and 6 in axial directions. Figure 2 displays a graphical schema of the textures configuration on the bearing wall. The ratio of depth (Dt) to width (Wt) of the textures is 0.5 and fixed for all textures. In this study, the Dt varies between 0.5, 1, and 1.5 mm, and each geometry is simulated under different regions on bearing surface, which are determined by the starting angle (α).

The bearing surface is divided into three primary regions. As the lubricant arrives at the converging area (80-160), the generated pressure begins to rise and reaches its peak value in the high-pressure area (160-240), where the pressure generated in this area isolates the bearing from the journal and counteracts the applied loads exerted on the journal. However, as

the lubricant arrives in the divergent area (240-320), the lubricant pressure decreases and falls below saturation pressure, and cavitation occurs.

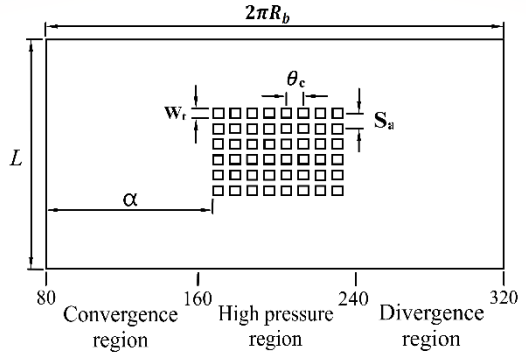

Fig. 2. Geometry of textured bearing surface

Table 1. Dimensions of the JB model

Symbol	Parameters	Values
R_{bi}	Bearing inside radius	15 mm
R_{bo}	Bearing Outside radius	17 mm
L	Bearing Length	20 mm
R_S	Radius of shaft	14.97 mm
e	Eccentricity	0.018 mm
ε	Eccentricity ratios	0.1-0.9
θ	Attitude angle	45 °
θ_c	Circumference spacing of texture	10 °
S_a	Axial spacing of texture	2.8 mm
N	Rotating speed	600 rpm
α	Starting angle	80 °, 160 °, 240 °

2.2. Boundary conditions

The analysis is accomplished assuming steady-state conditions, operating pressure 101325 Pa, zero gravity and external force. The two surfaces of the lubricant domain are modelled as static and moving walls with no slipping velocity, respectively, while the two sides are modelled as inlet and outlet, as presented in Figure 3.

The inlet and outlet are simulated as inlet and outlet pressure with gauge pressures of 150 kPa and 100 kPa, respectively. The bearing domain was considered deformable (made from copper) and fixed from the outer surface. In the Fluent system, the smoothing mesh technique was used to create a coupling system for the surfaces of the lubricant domain, while in the Static Structural system; a fluid-solid interface was created for the surface of the solid domain. Therefore, the fluid-solid interface connects the surfaces of the lubricant and solid domains. The pressure-based solution is employed for the numerical examination. The SIMPLEC process is employed for the velocity and pressure equation coupling, whereas the others remain default. Convergence standards of 10-6 are assumed for the residual terms. The physical characteristics of the lubricant and solid domain are listed in Table 2

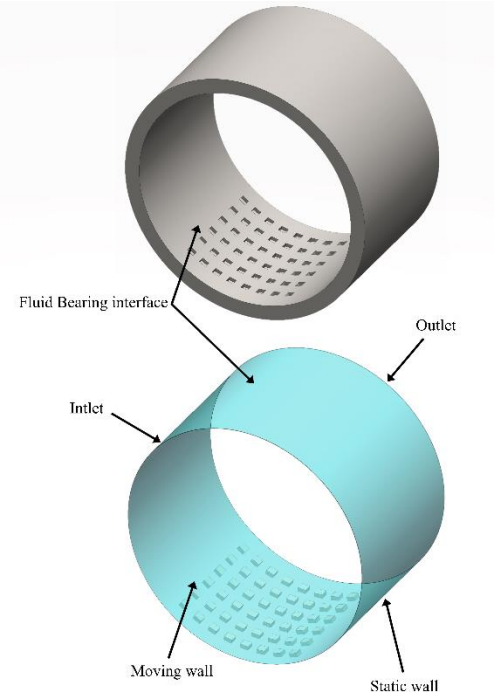

Fig. 3. Journal bearing model: description of domain surfaces

.

Table 2. Physical properties of the lubricant and bearing material

Symbol	Parameters	Values
ρl	Density of lubricant	822 kg.m^{-3}
ρv	Density of vapour	1.29 kg.m^{-3}
μl	Viscosity of lubricant	0.037 Pa.s
μv	Viscosity of vapour	5.953×10^{-6} Pa.s
ρb	Density of bearing	8.935 g.cm^{-3}
E	Modulus of elasticity	128 GPa
υ	Poisson ratio	0.34

2.3. Meshing procedure

A mesh analysis was conducted to determine the final mesh parameters. Each of the two domains was assigned a structured mesh with 140 elements in the tangential and 100 in the axial directions. Additionally, 10 layers of elements were assigned in lubrication thickness and Dt and 20 layers of elements in bearing thickness. The Solid226 element was utilized in all two domains. Figure 4 illustrates the mesh used. The mesh independence outcomes are reported in Table 3. It was observed that the differences in LCC were minimal when the mesh numbers for lubricant and solid were 279087 and 270891, respectively. Therefore, a mesh number of 549,978 was selected for this analysis.

Table 3. Mesh independence of the simulation model

Fluid domain elements	Solid domain elements	LCC (N)	Deviation (%)
178335	165785	307.14	1.12
198053	186246	307.98	0.95
223146	213421	308.78	0.69
256831	245974	309.25	0.54
279087	270,891	310.91	0

2.4. Elastic hydrodynamic modelling procedure

The textured JB models were simulated using Ansys Fluent and Mechanical Structure systems. A two-way coupling system was employed to link the fluid and solid domains, where the Fluent and Mechanical Structure systems exchanged data in both domains for pressure continuity and mesh displacement. Specifically, the pressure field data from Fluent to the Mechanical Structure system and the mesh displacement of the interface were transferred from the FE to the fluent system. The algorithm used to calculate the bearing properties is shown in Figure 5.

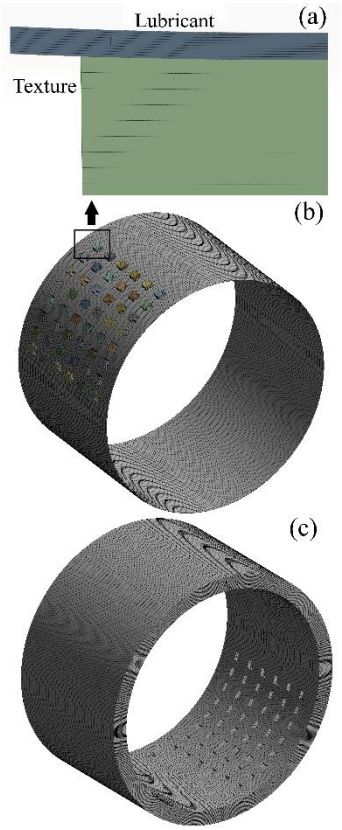

Fig. 4. Mesh details of the two domain: (a) Detail of the lubricant and texture mesh, (b) Lubricant mesh, (c) Bearing mesh

The elastic hydrodynamic model is solved through several steps, which are presented below:

1. In the first stage, the lubricant flow characteristics are estimated using a fluent system.
2. The calculated pressure profile of the lubricant is moved to the FE solver through the fluid/solid interface to calculate the mesh displacement caused by mechanical deformation on the solid domain.
3. The mesh displacement is then transferred to a fluent solver to update the geometry of the bearing surface.
4. This procedure is repeated until convergence is achieved.
5. Finally, all the static properties of the bearing are calculated.

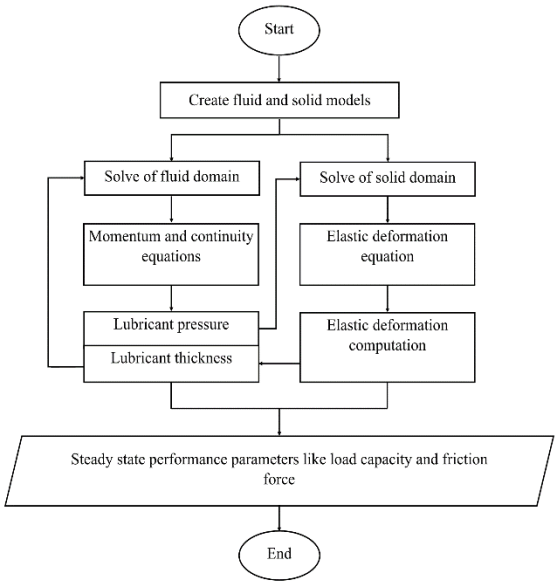

Fig. 5. Elastic hydrodynamic analysis of JB: Calculation algorithm

2.5. Governing equation

In Fluent, the performance of the fluid domain is predicted using conservation equations for mass and momentum. The conservation equations are written assuming the flow is incompressible, laminar, has zero gravity and external force, and operates under steady-state conditions [23].

$$\nabla \cdot v = 0 \tag{1}$$

$$\rho_f \nabla(v \cdot v) - \nabla\bar{\tau} = -\nabla P \tag{2}$$

$$\bar{\tau} = \mu_f \left[(\nabla v + \nabla v^T) - \frac{2}{3}\nabla v I\right] \tag{3}$$

Variables μ_f, ρ_f, I, P, and $\bar{\tau}$ represent the fluid viscosity, fluid density, unit tensor, static pressure, and stress tensor, respectively.

In the cavitation zone, the transfer of mass can be computed by utilizing the vapour transport equation presented below [24]:

$$R_b \frac{d^2 R_b}{dt^2} + \frac{3}{2}\left(\frac{dR_b}{dt}\right)^2 + \frac{2\sigma}{\rho_f R_b} = \frac{P_g - P}{\rho_f} \tag{4}$$

Variables R_b, P_g, and σ represent the bubble radius, bubble pressure, and surface tension coefficient, respectively. Ignoring the second-order terms and surface tension, equation (4) reduces to the following expression:

$$\frac{dR_b}{dt} = \sqrt{\frac{3}{2}\frac{P_v - P}{\rho_f}} \tag{5}$$

Then the total interphase mass transfer rate per unit volume is:

$$\dot{m}_{fg} = F\frac{3r_{nuc}(1-r_g)\rho_g}{R_{nuc}}\sqrt{\frac{3}{2}\frac{|P_v - P|}{\rho_f}}sgn(P_v - P) \tag{6}$$

Variables R_{nuc}, r_g, ρ_g, and r_{nuc} represent the nucleation site radius, bubble volume fraction, vapor density, and nucleation sites volume fraction, respectively. The default model parameters for the Rayleigh-Plesset cavitation method in Fluent are $R_{nuc} = 10^{-6}$, $r_{nuc} = 5\times10^{-4}$, $F_{vap} = 50$, $F_{cond} = 0.01$.

In the current examination, the regression method presented by [25] is used to calculate the values of viscosity of lubricants with weight

concentration of AL2O3 nano additives ranging from 0.1% to 0.5%. The regression method is achieved by maintaining the viscosity and temperature as dependent variables, while the wt. % of AL2O3 nanoparticles is an independent variable. According to the results of scanning electron microscopy performed by [25], the size, shape, and spreading of the AL2O3 nanoparticles were spherical and evenly spread in the lubricant with an even size of 30 nm. The values of viscosity of lubricant with AL2O3 nano additive are computed by [25]:

$$\mu = \mu_o e^{\left(K_1 - K_2 \frac{T}{T_o}\right)} \tag{7}$$

Where:

$$K_1 = 1.142 - 0.804 w_t + 3.974 {w_t}^2 - 5.691 {w_t}^3 \tag{8}$$

$$K_2 = 1.163 - 1.041 w_t + 4.218 {w_t}^2 - 5.08 {w_t}^3 \tag{9}$$

Equation (7), (8), and (9) were written in C language using the DEFINE PROPERTY macro and then, included in the analysis using a user-defined function (UDF).

AL2O3 nano additive was selected in this study for its ability to form a protective layer that repairs the worn surface as it accumulates with the metal debris in valleys, smoothing it and decreasing the coefficient of friction [26].

The LCC and FF can be acquired by integrating the pressure and viscosity shear force, respectively, over the journal surface as follows [24]:

$$LCC = \int_0^L \int_0^{2\pi} P R_s \, d\theta dz \tag{10}$$

$$FF = \int_0^L \int_0^{2\pi} \tau R_s \, d\theta dz \tag{11}$$

The equilibrium of the bearing domain is governed by the second law of motion given below [27]:

$$\rho_b \ddot{d}_s = \nabla \cdot \sigma_b + f_b \tag{12}$$

Variables ρ_b, $\ddot{d}_b$, σ_b, and f_b represent the bearing density, local acceleration, stress tensor, and body force, respectively.

The lubricant pressure deforms the bearing surface, altering the boundary condition at the interface between lubricant and bearing. Deformation compatibility and traction balancing are represented by the nodes at the interface of the lubricant and bearing:

$$\begin{cases} d_f = d_b \\ n \cdot \tau_f = n \cdot \tau_b \end{cases} \tag{13}$$

Variables d_f and τ_f represent the displacement and stress of lubricant domain, and d_b and τ_b represent the displacement and stress of bearing domain.

The direct method is used to solve fluid solid interaction (FSI) models by combining equations of the lubricant and bearing domains into a matrix given below [27]:

$$\begin{bmatrix} A_{ff} & A_{fb} \\ A_{bf} & A_{bb} \end{bmatrix} \begin{bmatrix} \Delta X_f^k \\ \Delta X_b^k \end{bmatrix} = \begin{bmatrix} F_f \\ F_b \end{bmatrix} \tag{14}$$

Variables A_{ff}, A_{bb}, A_{fb}, and A_{bf} represent the fluid matrix, bearing matrix, and coupling effects matrix correspondingly. F_f and F_b represent force vectors in the fluid and bearing domain correspondingly. ΔX_f^k and ΔX_s^k are the solutions for both domains, whereas k is the iteration number.

2.6. Validation

The FSI model is validated at elastic bearing conditions in this study, specifically for a plain JB. The validation process involves analysing the simulation results for rigid and elastic bearing conditions, depicted in Figure 6(a).

The results show that the development of fluid pressure on the rigid bearing is greater in comparison with that of the elastic bearing. The pressure profile is compared with experimental data from the reference [22] under the same input parameters and boundary conditions to validate the simulation results, as depicted in Figure 6(b). The maximum pressure difference between the simulation and experimental results is only 2.81%, indicating a good agreement between the two data sets.

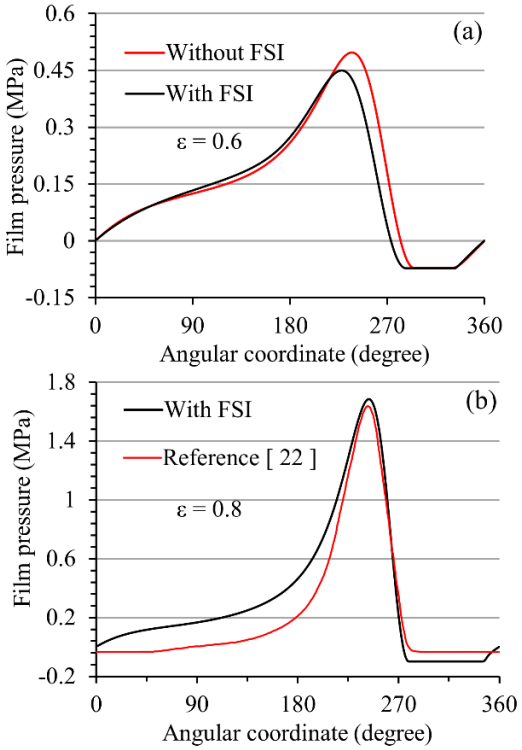

Fig. 6. Validation of present work with the data from reference [22]

3. RESULTS AND DISCUSSION

The properties of the JB like LCC and FF are determined by considering the texture of the rectangular shape in convergence region, high-pressure region, and divergence region using the FSI method. The JB characteristics are calculated with ε of 0.1 to 0.9, and the Dt ranges from 0.5 mm to 1.5 mm for different regions to obtain the optimum values in a particular region by comparing its characteristics. AL2O3 nanoparticles were added into the lubricant in the highest performance region to find its effect on JB performance. It should be noted that all the LCC and FF values that will be

analysed in the results are the total values of the bearing. Below are the main results of this study:

3.1. Influence of Dt and ε Convergence region

In this region, both textured and untextured bearings show an increase in LCC with an increase in ε from 0.1 to 0.9. The maximum LCC is observed in the case of untextured bearings. However, in the case of textured bearings, the LCC decreases as the Dt increases from 0.5 to 1.5 mm. Figure 7(a) illustrates that the percentage reduction in LCC is 35.08 % at a lower ε of 0.1 and 19.62 % at a higher ε of 0.9 with a Dt of 1.5 mm, compared to the untextured bearings.

The FF decrease with increasing ε from 0.1 to 0.9 for textured and untextured bearings. The FF is minimal in the case of untextured bearings. However, in the case of texture bearings, the FF increases as the Dt increases for a certain ε, as depicted in Figure 7(b). The FF is increased by 10.84 % at a lower ε of 0.1 and by 25.17 % at a higher ε of 0.9 compared to the untextured bearings with a Dt of 1.5 mm. Figure 8 shows the lubricant field contours at ε of 0.6 for the textured bearings. The intensity of streamlines of the lubricant flow field becomes stronger as Dt increases. In addition, the vortex radius in the lubricant flow field is the smallest at Dt = 1.5 mm, indicating that the laminar flow condition of the lubricant is predominant. The vortex is generated primarily by the inertial influence of the lubricant flow within the texture area. Consequently, more lubricant flows into the texture area, causing the pressure to decrease, as shown in Figures 9(a) and 9(b), resulting in a reduction in the LCC and a rise in the FF.

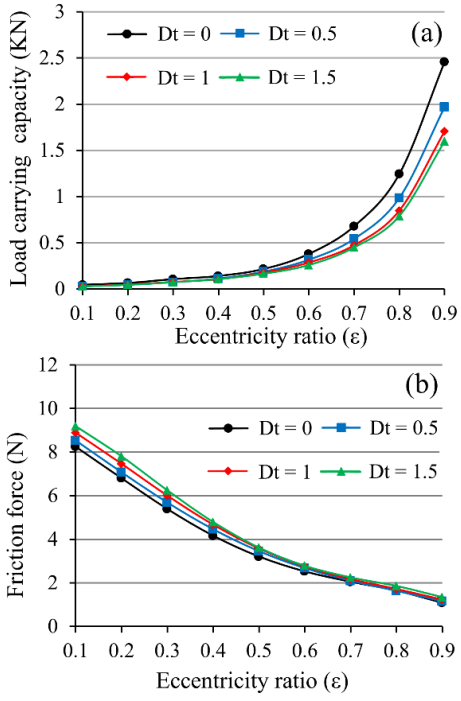

Fig. 7. Variation of JB characteristics in the convergence region (a) LCC and (b) FF

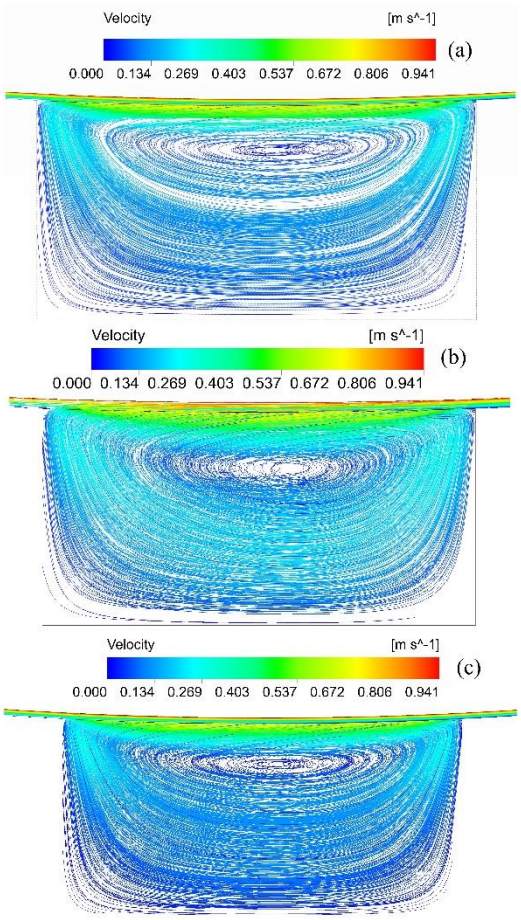

Fig. 8. Lubricant field contour of textured area in the convergence region at ε of 0.6 and Dt of (a) 0.5, (b) 1, and (c) 1.5 mm.

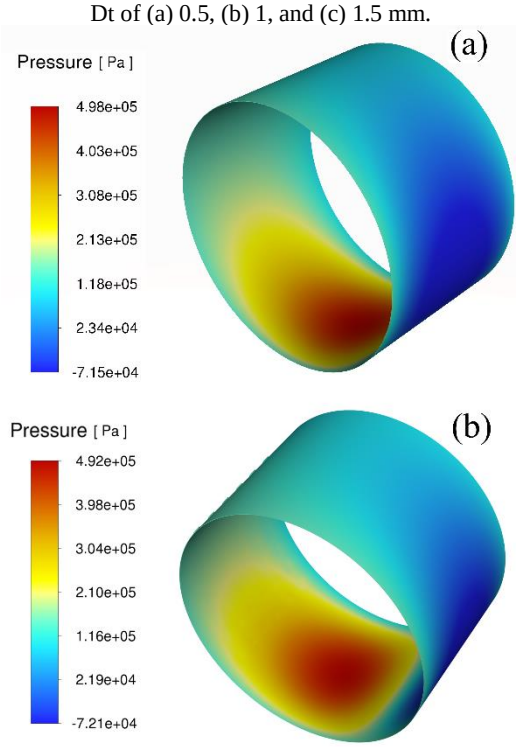

Fig. 9. Pressure contour of (a) untextured bearing and (b) convergence region of the bearing at ε 0.6 and Dt of 0.5

Divergence region

In this region, both textured and untextured bearings show an increase in LCC with an increase in ε from 0.1 to 0.9. The maximum LCC is observed in the case of untextured bearings. However, in the case of textured bearings, the LCC decreases as the Dt increases from 0.5 to 1.5. Figure 10 (a) shows that the LCC is reduced by 35.98 % at a lower ε of 0.1 and 24.56 % at a higher ε of 0.9, compared to the untextured bearings with a Dt of 1.5 mm. However, the reduction in LCC is 0.9 % higher compared to the convergence region for the same ε and Dt. FF decrease with increasing ε from 0.1 to 0.9 for textured and untextured bearings. The FF is minimal in the case of untextured bearings. However, in the case of texture bearings, the FF increases as the Dt increase for a certain ε, as depicted in Figure 10 (b). The FF is increased by 23.07 % at a lower ε of 0.1 and 47.33 % at a higher ε of 0.9 compared to the untextured bearings with a Dt of 1.5 mm. In addition, at the same ε and Dt, the increase in FF within this region is 12.23 % higher than the increase observed when texturing in the convergence region. Figure 11 show the pressure contour at ε 0.6 for the textured bearing.

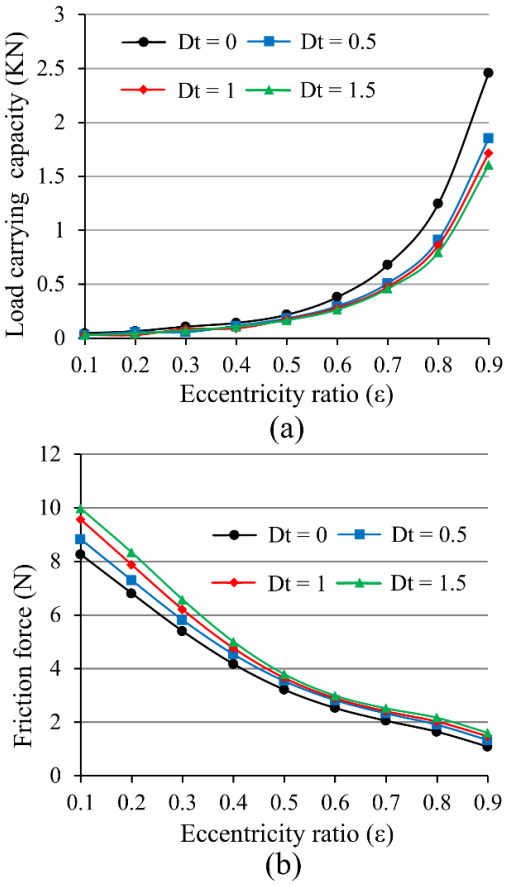

Fig. 10. Variation of JB characteristics in the divergence region (a) LCC and (b) FF

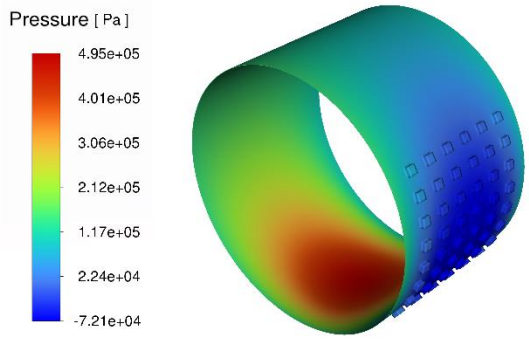

Fig. 11. Pressure contour of divergence region of the bearing at ε 0.6 and Dt of 0.5 mm

High pressure region

The LCC significantly increases in this region compared to the converging and diverging regions. As the ε increases from 0.1 to 0.9, the LCC increases. For a Dt of 0.5 mm, the LCC is increased by 16.51 % at a ε ratio of 0.1. However, at a higher ε of 0.9, there is a 15.87% reduction in LCC compared to the nontextured bearings, as displayed in Figure 12(a). Nonetheless, for ε from 0.1 to 0.7, the LCC value increases with a Dt of 0.5 mm but then decreases as the Dt and ε increase.

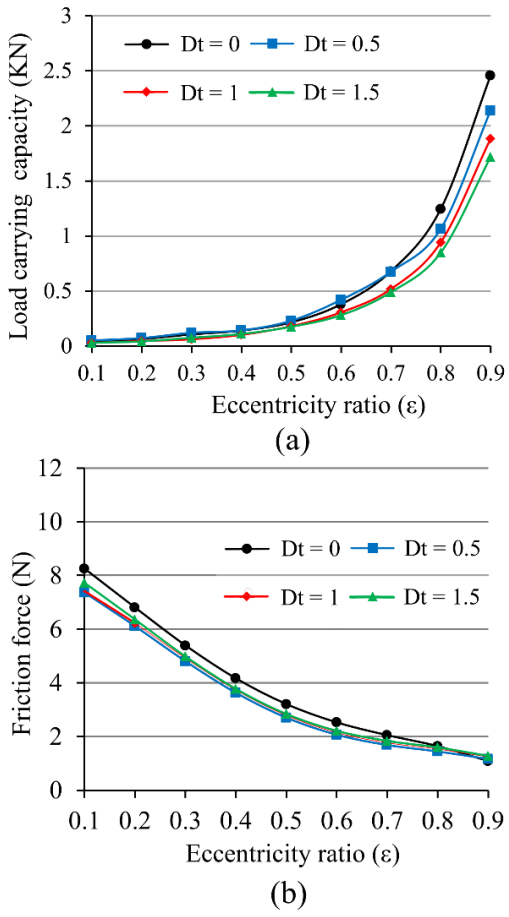

Fig. 12. Variation of JB characteristics in the high-pressure region (a) LCC and (b) FF

The value of FF decreases when the ε increases from 0.1 to 0.9 for textured and untextured bearings.

At a ε ratio of 0.1, the FF is decreased by 12.96 %, while at a higher ε of 0.9; there is a 55.4% increase in the FF corresponding to a Dt of 0.5 mm, as depicted in Figure 12(b). This is because when texture is applied to high-pressure region, the journal acquires additional area to move toward the bearing area. This results in a decrease in the thickness of the lubricant layer, which can cause a rise in the pressure value and LCC and a reduction in FF. Figure 13 displays the pressure contours at ε 0.6 and a Dt of 0.5 mm.

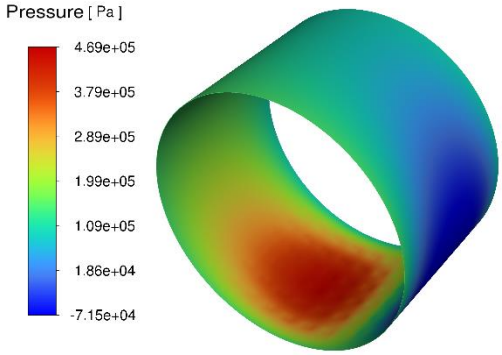

Fig. 13. Pressure contour of high-pressure region of the bearing at ε 0.6 and Dt of 0.5 mm

3.2. Influence of AL2O3 nanoparticles

According to Kalakada et al. [25], adding AL2O3 nanoparticles to lubricants has improved the performance of JB. AL2O3 nanoparticles are incorporated into the high-pressure region of the bearing to enhance its performance further, as this region provides the highest LCC and minimal FF of bearings with textures. The viscosity of AL2O3 nanoparticles is calculated for a weight fraction of 0.1–0.5%. The analyses is conducted at ε of 0.1 and Dt of 0.5 mm, as the highest LCC and minimal FF have been achieved at these values without adding AL2O3 nanoparticles to the lubricant.

Figure 14 illustrates the significant improvement in LCC at higher weight fractions of AL2O3 nanoparticles. FF decreases with an increase in lubricant additive weight fraction. The addition of AL2O3 nanoparticles at a weight fraction of 0.5% results in a 40.87 % improvement in LCC and 29.5 % reduction in FF compared to the plain bearing. Additionally, there is a 20.6 % increase in LCC and 21 % decrease in FF compared with without adding AL2O3 nanoparticles to lubricants in the high-pressure region with texturing.

Figure 15 displays the variation of lubricant flow rate with wt. % of AL2O3 nanoparticles. The results show that as the wt. % of AL2O3 nanoparticles increases, the lubricant flow rate decreases. This is because the addition of AL2O3 nanoparticles leads to an increase in the lubricant viscosity, which rises the resistance existing by the viscous force, thereby reducing the flow ability. Consequently, increasing the wt. % of AL2O3 nanoparticles in the lubricant increases the LCC and reduces the FF.

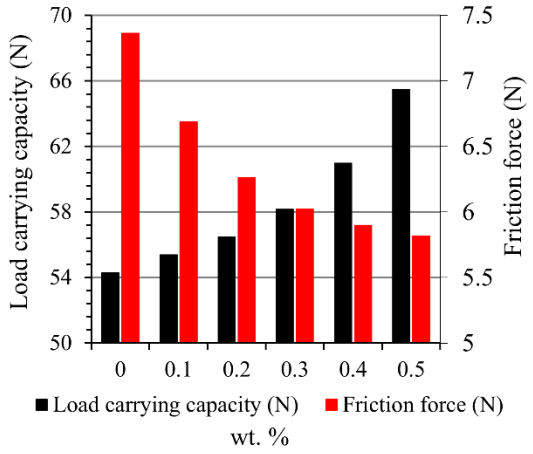

Fig. 14. Variations of LCC and FF with wt. % of AL2O3 nanoparticles at ε of 0.1 and Dt of 0.5 mm in the high-pressure region

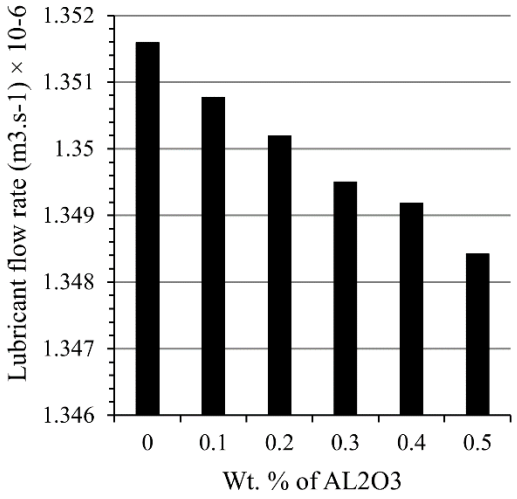

Fig. 15. Variations of lubricant flow rate with wt. % of AL2O3 nanoparticles at ε of 0.1 and Dt of 0.5 mm in the high-pressure region

3.3. Influence of bearing deformation

The pressure of the lubricant film in a JB causes elastic deformation of the bearing. The bearing's characteristics was examined while considering the elastic deformation to understand the impact of elastic deformation.

When comparing the pressure profiles of textured bearings in Figure 16, it was observed that elastic deformation causes a reduction in lubricant pressure, which is particularly noticeable in the high-pressure region. Table 4 displays the LCC of the bearing in two cases. Compared to the case without considering elastic deformation, the LCC values decrease when elastic deformation is considered. Figure 17 displays the deformation contour at ε 0.6 and a Dt of 1.5 mm. The generated deformation of the bearing causes a rise in lubricant thickness compared to the original convergence effect of JB, which interrupts pressure accumulation and reduces the maximum pressure; the lower maximum pressure leads to a reduced whole pressure integral and, consequently, a lower value of LCC.

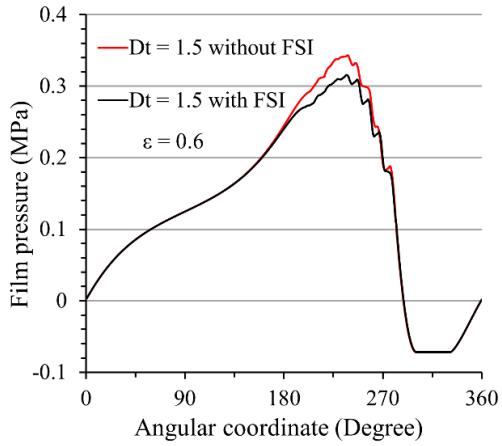

Fig. 16. Pressure profiles of textured bearings

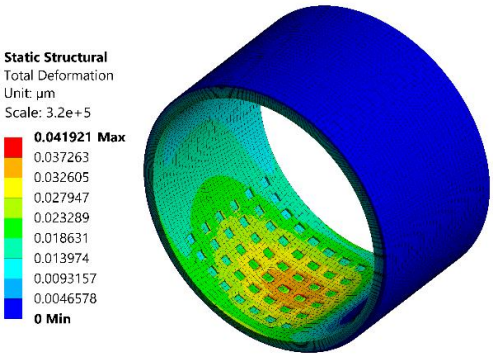

Fig. 17. Deformation contour of JB at ε of 0.6 and Dt of 1.5 mm in the high-pressure region.

Table 4. Bearing performance of two cases

	LCC (N)	
Eccentricity ratio	With FSI	Without FSI
0.1	54.3	57.5
0.2	75.7	80.7
0.3	123.8	132.1
0.4	145.3	153.9
0.5	233.1	248.2
0.6	422.3	439.3
0.7	676.8	698.7
0.8	1066.8	1113.6
0.9	2139.3	2209.4

4. CONCLUSION

In this research, the influence of rectangular form textures in convergence, divergence, and high-pressure regions of the bearing surface was analysed to investigate the static properties of a JB using the FSI method. After achieving the highest improvement of characteristics parameters in terms of LCC and FF in a specific region, AL2O3 nanoparticles are added at a weight fraction of 0.1-0.5% in the base lubricant to enhance the bearing's properties further. Based on the outcomes of the entire investigation, the following conclusions are drawn:

1. The highest rise of LCC of 16.51 % and a reduction of 12.96 % of the FF is noted in the high-pressure region, corresponding to ε of 0.1 and Dt of 0.5 mm without adding AL2O3 nanoparticles in the lubricants.
2. After adding AL2O3 nanoparticles in the lubricant, an additional increase of LCC is noted to be highest at a wt. % of 0.5 by 40.87 % compared with the untextured bearing and 20.6 % compared with the highest value acquired without adding AL2O3 nanoparticles in the high-pressure region with textures.
3. The results of the FSI analysis indicate that bearing deformation has a considerable impact on the characteristics of JB. It causes a reduction in both the lubricant pressure and the LCC.

Source of funding: *This research received no external funding.*

Author contributions: *research concept and design, M.R.H.; Collection and/or assembly of data, M.R.H., A.A.T.; Data analysis and interpretation, M.R.H., S.A.A., M.A.M.; Writing the article, M.R.H., S.A.A.; Critical revision of the article, M.R.H., H.H.H., A.A.T., M.A.M.; Final approval of the article, M.R.H., H.H.H.*

Declaration of competing interest: *The authors declare that they have no known competing financial interests or personal relationships that could have appeared to influence the work reported in this paper.*

REFERENCES

1. Rao T, Rani AMA, Nagarajan T, Hashim FM. Analysis of slider and journal bearing using partially textured slip surface. Tribology International 2012;56: 121-128. https://doi.org/10.1016/j.triboint.2012.06.010.
2. Ganji TS, Kakoty SK, Pandey RK. Analysis on micro elliptical textured journal bearing. International Journal of Current Engineering and Technology 2014; 2(2): 648-650. http://Dx.Doi.Org/10.14741/Ijcet/Spl.2.2014.123.
3. Shinde A, Pawar P, Shaikh P, Wangikar S, Salunkhe S, Dhamgaye V. Experimental and numerical analysis of conical shape hydrodynamic journal bearing with partial texturing. Procedia Manuf 2018; 20: 300–310. https://doi.org/10.1016/j.promfg.2018.02.045.
4. Sharma S., Jamwal G. Awasthi, RK. Enhancement of steady state performance of hydrodynamic journal bearing using chevron-shaped surface texture. Proceedings of the Institution of Mechanical Engineers, Part J: Journal of Engineering Tribology 2019); 233(12): 1833-1843. https://doi.org/10.1177/1350650119847369.
5. Tala-Ighil N, Maspeyrot P, Fillon M. Effects of surface texture on journal-bearing characteristics under steady-state operating conditions. Proceedings of the Institution of Mechanical Engineers, Part J: Journal of Engineering Tribology 2007; 221(6): 623-633. https://doi.org/10.1243/13506501JET287.
6. Buscaglia GC, Ciuperca I. Jai M. The effect of periodic textures on the static characteristics of thrust bearings. Journal of Tribology 2005; 127: 899-902. https://doi.org/10.1115/1.2033896.
7. Zhang Y, Chen G. Wang L. Effects of thermal and elastic deformations on lubricating properties of the

textured journal bearing. Advances in Mechanical Engineering 2019; 11(10): 1687814019883790. https://doi.org/10.1177/1687814019883790.
8. Niu Y, Hao X, Xia A, Wang L, Liu Q, Li L. He N. Effects of textured surfaces on the properties of hydrodynamic bearing. The International Journal of Advanced Manufacturing Technology 2022; 118: 1589-1596.https://doi.org/10.1007/s00170-021-08022-1.
9. Yu R, Li P. Chen W. Study of grease lubricated journal bearing with partial surface texture. Industrial Lubrication and Tribology 2016; 68(2): 149-157. https://doi.org/10.1108/ILT-03-2015-0028.
10. Manser B, Belaidi I, Hamrani A, Khelladi S. Bakir F. Texture shape effects on hydrodynamic journal bearing performances using mass-conserving numerical approach. Tribology-Materials, Surfaces & Interfaces 2020; 14(1): 33-50. https://doi.org/10.1080/17515831.2019.1666232.
11. Kango S, Singh D. Sharma RK. (2012). Numerical investigation on the influence of surface texture on the performance of hydrodynamic journal bearing. Meccanica 2012; 47: 469-482. https://doi.org/10.1007/s11012-011-9460-y.
12. Babu KS, Nair KP, Rajendrakumar PK. Computational analysis of journal bearing operating under lubricant containing Al2O3 and ZnO nanoparticles. International Journal of Engineering, Science and Technology 2014; 6(1): 34-42. https://doi.org/10.4314/ijest.v6i1.4.
13. Binu KG, Shenoy BS, Rao DS, and Pai R. A variable viscosity approach for the evaluation of load carrying capacity of oil lubricated journal bearing with TiO2 nanoparticles as lubricant additives. Procedia Materials Science 2014; 6: 1051-1067. https://doi.org/10.1016/j.mspro.2014.07.176.
14. Dang RK, Chauhan A. Dhami SS. Static thermal performance evaluation of elliptical journal bearings with nanolubricants. Proceedings of the Institution of Mechanical Engineers, Part J: Journal of Engineering Tribology 2021; 235(8):1627-1640. https://doi.org/10.1177/1350650120970742.
15. Sia SY, Bassyony EZ. Sarhan AA. Development of SiO2 nanolubrication system to be used in sliding bearings. The International Journal of Advanced Manufacturing Technology 2014; 71: 1277-1284. https://doi.org/10.1007/s00170-013-5566-9.
16. Gundarneeya TP, Vakharia DP. Performance analysis of journal bearing operating on nanolubricants with TiO2, CuO and Al2O3 nanoparticles as lubricant additives. Materials Today: Proceedings 2021;45: 5624-5630. https://doi.org/10.1016/j.matpr.2021.02.350.
17. Nair PK, Ahmed MS, Al-qahtani ST. Static and dynamic analysis of hydrodynamic journal bearing operating under nano lubricants. International Journal of Nanoparticles 2009; 2(1-6): 251-262. https://doi.org/10.1504/IJNP.2009.028757.
18. Yathish K, Binu KG, Shenoy BS, Rao DS, Pai R. Study of TiO2 nanoparticles as lubricant additive in two-axial groove journal bearing. International Journal of Mechanical, Aerospace, Industrial and Mechatronics Engineering 2014; 8(11): 1723-1729. https://doi.org/10.5281/zenodo.1096705.
19. Suryawanshi SR, Pattiwar JT. Effect of TiO2 nanoparticles blended with lubricating oil on the tribological performance of the journal bearing. Tribology in Industry 2018; 40(3): 370-391. https://doi.org/10.24874/ti.2018.40.03.04.
20. Bhattacharjee B, Chakraborti P, Choudhuri K. Nano-fluid lubrication of single-layered porous hydrostatic bearing: a theoretical approach. Journal of the Brazilian Society of Mechanical Sciences and Engineering 2020; 42(7): 1-9. https://doi.org/10.1007/s40430-020-02446-8.
21. Sadabadi H, Sanati Nezhad A. Nanofluids for performance improvement of heavy machinery journal bearings: a simulation study. Nanomaterials 2020; 10(11): 2120. https://doi.org/10.3390/nano10112120.
22. Gao G, Yin Z, Jiang D, Zhang X. Numerical analysis of plain journal bearing under hydrodynamic lubrication by water. Tribology international 2014; 75: 31-38. https://doi.org/10.1016/j.triboint.2014.03.009.
23. Greenshields CJ, Weller HG. Notes on Computational Fluid Dynamics: General Principles. CFD Direct Limited: Reading, UK; 2022.
24. Dhande DY, and Pande DW. Numerical analysis of multiphase flow in hydrodynamic journal bearing using CFD coupled Fluid Structure interaction with cavitation. IEEE 2016. https://doi.org/10.1109/ICACDOT.2016.7877731.
25. Kalakada SB, Kumarapillai PNN, PK RK. Static characteristics of thermohydrodynamic journal bearing operating under lubricants containing nanoparticles. Industrial Lubrication and Tribology 2015; 67(1): 38-46. https://doi.org/10.1108/ILT-01-2013-0015.
26. Ghalme S, Koinkar P, Bhalerao YJ. Effect of aluminium oxide (Al2O3) nanoparticles addition into lubricating oil on tribological performance. Tribology in Industry 2020; 42(3): 494-502. https://doi.org/10.24874/ti.871.04.20.07.
27. Lin Q, Bao Q, Li K, Khonsari MM, Zhao H. An investigation into the transient behavior of journal bearing with surface texture based on fluid-structure interaction approach. Tribology international 2018; 118: 46–255. https://doi.org/10.1016/j.triboint.2017.09.026.

Mohanad R. HAMEED
University of Babylon, Institution of Engineering/
Al-Musayab, Iraq
e-mail: msb.mohanad.ramadhan@uobabylon.edu.iq

Sarmad A. ALI
University of Babylon, Institution of Engineering/
Al-Musayab, Iraq
e-mail: sarmad.ahmed96@uobabylon.edu.iq

Hamid H. HADWAN
University of Babylon, Institution of Engineering/
Al-Musayab, Iraq
met.hamed.huss@uobabylon.edu.iq

Ahmed A. TOMAN
University of Babylon, Institution of Engineering/
Al-Musayab, Iraq
e-mail: ahmed.toman@uobabylon.edu.iq

Mushrek A. MAHDI
University of Babylon, Institution of Engineering/
Al-Musayab, Iraq
e-mail: msb.mushrek.alawi@uobabylon.edu.iq